# Electromagnetic properties of 3D-printed carbon-BaTiO 3 composites

Pauline Blyweert, Alexander Zharov, Darya Meisak, Artyom Plyushch, Jan Macutkevič, Jūras Banys, Vanessa Fierro, Alain Celzard

# Electromagnetic properties of 3D-printed carbon-$BaTiO_3$ composites

Pauline Blyweert[1], Alexander Zharov[1], Darya Meisak[2], Artyom Plyushch[2], Jan Macutkevič[2]*, Jūras Banys[2], Vanessa Fierro[1] and Alain Celzard[1,3]

[1]Physics faculty, Vilnius university, Sauletekio av. 9, Vilnius LT-10222, Lithuania
[2]Université de Lorraine, CNRS, IJL, 88000 Épinal, France
[3]Institut Universitaire de France (IUF), 75231 Paris, France
*jan.macutkevic@gmail.com

3D-printed carbon structures filled with $BaTiO_3$ nanoparticles were investigated in low (20 Hz – 1 MHz) and microwave (26 – 37 GHz) frequency ranges. These structures possess rather high electrical conductivity in the low-frequency range (about several S/cm) and excellent dielectric properties in the microwave range. The electrical transport is thermally activated and can be attributed to electron transport through various defects. The electromagnetic properties of the investigated structures in the microwave range are very attractive. For example, the absorption of a 2 mm-plate with 46 wt.% of $BaTiO_3$ at 30 GHz is 50%. The impact of $BaTiO_3$ nanoparticles on the dielectric properties of the hybrid structures is positive over a wide frequency range, and the highest dielectric losses are observed for structures with 46 wt.% $BaTiO_3$.

In the modern world, it is impossible to overestimate the significance of electromagnetic wave applications for society. Indeed, telecommunications and electronics, including cell phones, Wi-Fi and satellite broadcast systems, play an increasingly important role in our daily life. However, with the increase in the number of devices operating in close frequency ranges, the problem of electromagnetic interference becomes crucial. Moreover, this problem is exacerbated by the uncontrollable increase of the average power of microwave radiation required to transmit larger amounts of information, which represents a possible threat to human health. As a result, great efforts are currently being made to develop and improve microwave shielding and absorption technologies.

In terms of electromagnetic shielding applications, carbon-based materials, including carbon nanotubes, carbon black, carbon (nano)platelets, carbon (nano)fibers, and graphite, as well as polymer composites containing such fillers, are widely used due to their superior electrical properties, chemical inertness, light weight, and relatively low cost [1–5]. The high intrinsic electrical conductivity of some carbon allotropes allow them to be incorporated into a polymer matrix to effectively modify the complex electric permittivity of composites, thereby enabling the tuning of electromagnetic absorption properties. Indeed, such electromagnetic properties are observed in polymeric composites with various carbon inclusions above the percolation threshold. Therefore, the percolation threshold should be as low as possible to preserve the optimal mechanical and thermal properties of the polymer matrix.

Composites containing carbon nanotubes have very low percolation threshold values (sometimes less than 0.1 wt.%) [6,7]. However, very often the carbon nanotubes form aggregates within the polymer matrix and the percolation and overall dielectric properties of the composites are determined by the distribution of the carbon nanotubes. Composites with other carbon nano-inclusions (graphene, exfoliated graphite, onion-like carbon) can also have a very low percolation threshold value, similar to that observed in carbon nanotube composites [8,9]. On the other hand, highly conductive porous carbon structures such as carbon foams with typical pore sizes from one to several hundred micrometers and carbon gels with nano-sized pores were proposed as materials for electromagnetic shielding applications [10–14]. It has been shown that density is the key factor that determines the electromagnetic properties of these structures below 50 GHz, while the inner structure of the porous materials has an impact on the electromagnetic properties only in the terahertz frequency range [11].

Barium titanate ($BaTiO_3$, BT) exhibits three different phase transitions when the temperature is decreased: the first from cubic paraelectric to tetragonal ferroelectric phase at 398 K, the second from tetragonal to orthorhombic at 273 K, and the third from orthorhombic to rhombohedral at 183 K [15]. In its ferroelectric form, it is generally used in multilayer ceramic capacitors, nonlinear optic devices, thermistors, and electromechanical transducers [15]. Due to its high dielectric permittivity over a wide frequency range, BT has been proposed as filler in various composites for electromagnetic applications. In particular, BT nanoparticles (NPs) embedded in a polymer matrix, as well as several hybrid BT NP-containing nanocomposites, are reported to show excellent electromagnetic shielding properties [16–22]. Moreover, the addition of BT nanoparticles into composites based on carbon black [23], graphene [24], exfoliated graphite [25], and nanocarbon [26] has been claimed to enhance significantly the electromagnetic absorption in the resulting materials. Modification of carbon-based materials by various magnetically active addition is also a commonly accepted strategy [27,28]. It has been concluded that the addition of magnetic inclusions substantially improves the electromagnetic properties of carbon gels [27]. However, no broadband electromagnetic studies of carbon-based materials with ferroelectric inclusions have been performed to date. In the present study, we investigated the influence of the addition of BT NPs into different 3D-printed carbon structures on their electromagnetic absorption properties.

The carbon-$BaTiO_3$ composite samples were prepared by 3D printing followed by a heat treatment. A photocurable acrylate-tannin-$BaTiO_3$ resin was obtained by first mixing the photoinitiator BAPO (Phenylbis(2,4,6-trimethylbenzoyl)phosphine oxide, 0.3 wt.%, supplied by Lambson, Wetherby, England) with the aromatic acrylate oligomer CN154 CG, the aliphatic pentaerythritol tetraacrylate (PETA, SR295) and 1,6-Hexanediol diacrylate (HDDA, SR238), supplied by Sartomer (Arkema Group, Verneuil en Halatte, France) in a 4/4/2 ratio. Subsequently, tannin (25 wt.%) and $BaTiO_3$ nanoparticles (US Research Nanomaterials, purity 99.9%, particle size 200 nm, tetragonal structure, in weigh fractions $\phi_i$ = 0, 5, 10 or 15 wt.%) were added and stirred for a few minutes to ensure good dispersion in the resin. An initial concentration $\phi_i$ of $BaTiO_3$ nanoparticles higher than 15 wt.% caused a strong increase in the viscosity of the resin, preventing its 3D printing.

The resultant resins were processed in a DWS J28 desktop SLA (405 nm laser, DWS, Italy) to print cylinder (6.3 mm diameter and 8 mm height) and rods (1.33 mm diameter and 15.10 mm height). The printed structures were post-cured in a UV oven (405 nm) for 20 min at room temperature and finally converted into highly disordered carbon materials under pure nitrogen in a tubular furnace with a heating ramp of 1 °C/min to a final temperature of 900 °C, which was maintained for 1 hour. More information about the preparation method, schematized in Fig. 1a, and the main properties of the resultant carbon materials obtained this way can be found elsewhere [29, 30]). The structures sometimes warped a little during the pyrolysis, as shown in Fig. 1b, but it was always possible to obtain a very straight zone that matches the size of the waveguide (around 2.6 mm in height, which sometimes meant having to abrade the sample a little). The linear shrinkage was around 25% in all directions, without observed influence of the presence or concentration of BT particles.

During pyrolysis, the mass of $BaTiO_3$ remains constant, and as the carbon precursor is known to present a mass loss of about 80%, samples with a final content $\phi_f$ of 0, 20, 35 and 46 wt.% of $BaTiO_3$ in the carbon matrix were thus obtained. In the following, we will therefore only refer to these final concentrations of BT in the carbon, not to those, initial in the 3D printer resin. The dimensions of the samples were 6 mm diameter and 5 mm height for the cylinders, and 0.95 mm diameter and 10 mm height for the rods. Their characteristics in terms of bulk density and filler content are given in Table 1.

Table 1. $BaTiO_3$ weight fraction in composites before (initial) and after pyrolysis (final), and corresponding $BaTiO_3$ volume concentration and bulk density of carbon-based composites.

| Initial $BaTiO_3$ concentration, $\phi_i$, wt.% | Final $BaTiO_3$ concentration, $\phi_f$, wt.%* | Final $BaTiO_3$ concentration, $\Phi$, vol.%** | Bulk density, $\rho_b$, $g \cdot cm^{-3}$ |
|---|---|---|---|
| 0 | 0 | 0 | 0.42 |
| 5 | 20 | 2.5 | 0.73 |
| 10 | 35 | 5.3 | 0.89 |
| 15 | 46 | 7.9 | 1.01 |

* Calculated as $\phi_f = \phi_i / [(1-Y_C)\,\phi_i + Y_C]$, where $Y_C = 20.8\%$ is the carbon yield of the pure resin upon pyrolysis, i.e., $Y_C$ = final mass of carbon after pyrolysis / initial mass of resin [29].

** Calculated as $\Phi = \phi_f \times \rho_b / 6.02$, where 6.02 $g \cdot cm^{-3}$ is the density of bulk $BaTiO_3$.

SEM image of the fractured carbon-$BaTiO_3$ structure reveals a dispersion of $BaTiO_3$ in the porosity of the carbon matrix in the form of nanoparticles and some aggregates (Fig. 1c).

The electrical conductivity was measured at low frequency, i.e., between 20 Hz and 1 MHz, using a Hewlett-Packard 4284A LCR-meter. The measurements are based on the use of equivalent circuits to determine the complex impedance. From these quantities, the electrical conductivity was calculated according to the formula $\sigma = l/(S \cdot R)$, where $l$ and $S$ are the length and the cross-sectional area of the sample, respectively, and $R$ is the measured electrical resistance. The electrical conductivity was also investigated in the temperature range 120 – 300 K with a liquid nitrogen cryostat. Silver paint was used to make electrical contacts. The electromagnetic properties of the hybrid structures were also studied in the microwave frequency range (26–38 GHz, Ka-band) using a 7.2 × 3.4 $mm^2$ rectangular cross-section waveguide. An Elmika 2400 scalar network analyzer was

used to measure the scalar scattering parameters. Rod-like samples with a diameter of about 1 mm and a length of about 6 mm were investigated and placed in the center of the waveguide with their axis parallel to the electric field vector. All samples were glued to the sample holder with silver paint. The complex dielectric permittivity was calculated using a modified Newton optimization algorithm based on the microwave theory formalism (see [31] for details). This method is in good agreement with other microwave dielectric permittivity determination methods [31]. The measurements accuracy was ~10 %.

X-ray diffraction (XRD) analysis was performed on a DRON 3.0 diffractometer using Co Kα radiation (λ = 1.78896 Å), with a scan rate of 1.5 grad/s, a voltage of 35 kV, and a current of 20 mA. The COD database [32] was applied for identification.

The X-ray diffraction pattern of the 200-nm $BaTiO_3$ nanoparticles is shown in Fig. 2. All peaks are identified as P4mm $BaTiO_3$ (1507756) tetragonal phases. The reflections of the (002) and (200) planes of $BaTiO_3$ are clearly separated. This proves the ferroelectric tetragonal distortion of the $BaTiO_3$ crystal lattice.

The frequency dependencies of the electrical conductivity of the carbon structures with $BaTiO_3$ nanoparticles at room temperature are presented in Fig. 3a. It can be concluded that the electrical conductivity is almost independent of frequency and thus coincides with the DC conductivity. The conductivity values are moderately high (about several hundred S/m) and apparently depend on the amount of added $BaTiO_3$. In fact, this trend can be explained simply by the increase in density of the materials, as shown in Table 1. Structures with higher density should have higher electrical conductivity values [11]. However, another factor that may affect the electrical conductivity is the creation of electron donors or acceptors in the structures by the addition of $BaTiO_3$ [33]. Moreover, the addition of $BaTiO_3$, which is non-conductive, has very little effect on this trend since its volume fraction, which is the relevant quantity to explain the variation of electrical conductivity in these composites, remains quite low (see again Table 1). Indeed, because of its very high density (6.02 g $cm^{-3}$) compared to carbon (about 2 g $cm^{-3}$), the volume fraction of $BaTiO_3$ is much lower than its weight fraction.

The temperature dependence of DC electrical conductivity of the composite materials is presented in Fig. 3b. The electrical conductivity increases upon heating, as is typical for thermally activated electrical conductivity. The temperature dependence was fitted with Arrhenius's law separately below and above a certain critical temperature (solid lines in Fig. 3b):

$$\sigma = \sigma_0 e^{-\frac{E}{kT}} \quad (1)$$

where $\sigma_0$ is the pre-exponential factor, $E$ is the activation energy, and $k$ is the Boltzmann constant.

The obtained parameters are summarized in Table 2. The values of activation energies are similar to those obtained for carbon gels [13], therefore the electrical conductivity can be attributed to transport in the carbon matrix through various defects.

Table 2. Arrhenius law fitting parameters of the composite structures.

| $BaTiO_3$ concentration, $\phi_f$, wt.% | Temperature region, K | $\sigma_0$, S/cm | $E/k$, K (meV) |
|---|---|---|---|
| 0 | T < 155 | 7.2 | 137 (11.8) |
| | T > 155 | 9.6 | 184 (15.8) |
| 20 | T < 138 | 11.2 | 73 (6.3) |
| | T > 153 | 13.4 | 97.4 (8.4) |
| 35 | T < 161 | 11.2 | 103.5 (8.9) |
| | T > 161 | 13.8 | 136 (11.7) |
| 46 | T < 212 | 12.6 | 103 (8.9) |
| | T > 212 | 21.2 | 210 (18.1) |

The microwave spectra of the different structures are presented in Figs. 4 and 5. From Fig. 4a and 4b, it can be concluded that both real and imaginary parts of the complex dielectric permittivity strongly decrease with frequency according to Jonsher's universal power law. The values of the complex dielectric permittivity are quite high (ε' ≈ 10-30, ε'' ≈ 1-10), therefore it can be expected that these structures are suitable for electromagnetic shielding applications [34]. The dielectric losses ε'' are larger for structures with about 50 wt.% $BaTiO_3$ than for structures without $BaTiO_3$ (Fig. 4b and 4c). However, the impact of $BaTiO_3$ concentration on the dielectric permittivity of the structures is less pronounced, and only for the structure with a $BaTiO_3$ concentration of 20 wt.% is the dielectric permittivity slightly lower than for the other structures. The impact of $BaTiO_3$ on the dielectric properties of the structures is less marked with a carbon matrix than in polymer composites [16-23] due to shielding effect of free electrons in the carbon materials [27]. The dielectric dispersion of the materials in microwaves is caused by electron transport in the carbon matrix and is in good agreement with other carbon-based materials studied in microwaves [35]. In addition, and regardless of the BT concentration, the dielectric properties of the structures in the microwave frequency range are quite stable with temperature (Fig. 4d). A small increase of dielectric losses ε'' on cooling below 300 K is related to the electrical transport observed in Fig. 3b.

The scattering parameters of a standalone layer of the studied hybrid material in a free space can be calculated using the following equations [34]:

$$S_{11} = \frac{-j\left(\left({k_z}/{k_{2z}}\right)^2 - 1\right)\sin\left(k_{2z}\tau\right)}{2\,{k_{2z}}/{k_z}\cos(k_{2z}\tau) + j\left(\left({k_{2z}}/{k_z}\right)^2 - 1\right)\sin\left(k_{2z}\tau\right)}, \quad (2)$$

$$S_{21} = \frac{2\left({k_{2z}}/{k_z}\right)}{2{k_{2z}}/{k_z}\cos(k_{2z}\tau) + j\left(\left({k_{2z}}/{k_z}\right)^2 - 1\right)\sin\left(k_{2z}\tau\right)}, \quad (3)$$

where $k_z = 2\pi/\lambda$ and $k_{2z} = 2\pi\varepsilon^{0.5}/\lambda$ are the wavenumbers in the vacuum and sample's media, respectively, $\varepsilon$ is the measured permittivity of the composite, and $\tau$ is the thickness of the layer. The reflection, transmission, and absorption of the layer can be calculated as $R = |S_{11}|^2$, $T = |S_{21}|^2$, and $A = 1 - R - T$, respectively. The coefficient of absorption, which is defined as the ratio of the absorbed power to the incident power of the EM wave, does not represent the ability of the layer to absorb since part of the wave is already reflected at the interface and does not enter the layer. Due to this, the effective absorption coefficient, $A_{eff}$, can be defined as $A_{eff} = (1-R-T) / (1-R)$.

The microwave absorption properties of the hybrid structures, calculated using Eqs. (2, 3) and the measured complex permittivities (Fig. 4) for a 2-mm-thick plate, are shown in Fig. 5. It is clearly seen that for the whole frequency range, the trends are similar: small amounts of $BaTiO_3$ decrease the absorption, while as the BT concentration reaches 46 wt.%, the hybrid structures perform better than the control sample without BT.

At low concentrations of BT NPs, the absorption decreases with the addition of NPs. At the same time, [24–26] reported a sustained improvement in absorption properties with the addition of BT to composites. However, in the cited studies, BT NPs and different carbon structures were embedded in a polymer matrix, which significantly reduced the macroscopic conductivity of the composites. As a result, the microscopically conductive carbon nanostructures behaved as dielectric inclusions, as their typical size was much smaller than the electromagnetic scales, namely wavelength and skin depth. In contrast, in the composites studied here, the BT NPs were embedded in porous carbon, which made the samples macroscopically conductive. Consequently, the electromagnetic properties in the microwave range were dominated by the conductivity of the sample, at least for the lowest concentrations of BT. Therefore, the addition of small amounts of BT NPs decreased the absorption of the composites. Nevertheless, the results, both from measurements and calculations for 2-mm thick slabs at 30 GHz, show that the absorption of the most $BaTiO_3$ – loaded structures reaches 50%.

Another approach for shielding material applications is the $\lambda/4$ geometry known as the Salisbury screen [36]. A layer of dielectric material is placed on a back reflector, the incident irradiation reflects both from the first edge of the layer and from the back reflector. These two reflected waves interfere. If the phase difference is $\pi$, the interference causes the total reflected signal to be suppressed to 0%. The model is simple for the case of a lossless material ($\varepsilon'' = 0$). A simple resonant equation can be used to estimate the required layer thickness, which satisfies the condition of a totally reflection-free structure. However, for materials with complex dielectric permittivity, the situation is more complicated, since the wave reflected from the back-reflector undergoes an additional rotation of phase angle. As a result, only a particular combination of thickness, real and imaginary parts of the dielectric permittivity may satisfy the resonance condition at the selected frequency of the incident wave.

For the system with back reflector, the scattering parameter $S_{11}$ reads:

$$S_{11} = -\frac{k_z(exp\{2i\tau k_{2z}\} - 1) + k_{2z}(exp\{2i\tau k_{2z}\} + 1)}{k_z(1 - exp\{2i\tau k_{2z}\}) + k_{2z}(exp\{2i\tau k_{2z}\} + 1)} \quad (4)$$

As in Eq. (2,3), $k_z$ and $k_{2z}$ are the wavenumbers, $\varepsilon$ is the permittivity of the layer, and $\tau$ is the thickness. The dependence of $S_{11}$ (in dB) on thickness and frequency is presented in Fig. 6.

The presented materials show promise for Salisbury screen applications [36]. In particular, $S_{11}$ of the sample containing 46 wt.% $BaTiO_3$ is less than -40 dB, which corresponds to more than 99.99% of the incident irradiation. The intervals of frequency and thickness of the layer are narrow due to the resonant nature of the phenomenon. Literally, a tiny variation in thickness from 0.58 mm to 0.60 mm leads to the increase in $S_{11}$ from < -40 dB to > -20 dB. However, even if the system is far from resonance, attenuation of < -20 dB (or 99% of incident radiation) may be acceptable for a range of applications. In this case, the system can be applied as a band absorber in the 26-32 GHz range. However, this absorption range can be modified, as it has been previously shown that a small change in temperature (i.e., 5-7 K) can shift the position of the shielding efficiency peak of Salisbury screens ($SE_R=|20\log_{10}(S_{11})|$) [37]. As the $BaTiO_3$ concentration decreases, the system gradually goes out of resonance and $S_{11}$ increases. Finally, for the sample without $BaTiO_3$, the -20 dB level is unattainable.

In conclusion, carbon-$BaTiO_3$ composite samples were prepared by 3D printing of a mixture of photocrosslinkable resin and $BaTiO_3$ nanoparticles, followed by pyrolysis of the resulting preforms. The obtained structures exhibit a frequency-independent electrical conductivity value (about several S/cm) in the frequency range 20 Hz – 1 MHz, which is typical for glassy carbon. The temperature dependence of the DC conductivity follows the Arrhenius law, and the activation energies have values of about several meV, which is typical of electron transport through various defects. The addition of $BaTiO_3$ also increases the dielectric losses of the composite materials, while the dielectric permittivity is almost independent on $BaTiO_3$ concentration. Thus, we could observe that with 46 wt.% $BaTiO_3$ at 30 GHz, the electromagnetic absorption is 50%. Moreover, the microwave properties of the structures are stable over a wide temperature range, and only very small changes in the dielectric losses are related to electrical transport. Therefore, these structures, which can be prepared in any geometry since they are designed by laser stereolithography, can be considered for electromagnetic shielding applications.

This research received funding from Campus France and the Lithuanian Science Council through the joint program PHC Gilibert #46414VC “Hybrid gels for electromagnetic applications”. It was also sponsored by the NATO Science for Peace and Security Program (Grant G5697 CERTAIN “Globular carbon-based structures and metamaterials for enhanced electromagnetic protection”). The authors are grateful to Aliaksei Sokal for valuable discussion.

## References


1. F. Qin, C. A. Brosseau, Journal of Applied Physics **111**, 061301 (2012).

2. M.H. Al-Saleh, U. Sundararaj, Carbon **47**, 1738 (2009).

3. B. Wen, M. Cao, M. Lu, W. Cao, H. Shi, J. Liu, X. Wang, H. Jin, X. Fang, W. Wang, Adv. Mater. **26**, 3484 (2014).

4. X. Liu, Z. Zhang, Y. Wu, Composites Part B: Engineering **42**, 326 (2011).

5. G. Li, T. Xie, S. Yang, J. Jin, J. Jiang, J. Phys. Chem. C **116**, 9196 (2012).

6. J. K. W. Sandler, J. E. Kirk, I. A. Kinloch, M. S. P. Shaffer, A. H. Windle, Polymer **44**, 5893 (2003).

7. H. Deng, L. Lin, M. Ji, S. Zhang, M. Yang, Q. Fu, Progress in Polymer Science **39**, 627 (2014).

8. E. Palaimiene, J. Macutkevic, J. Banys, A. Selskis, V. Fierro, A. Celzard, S. Schaefer, O. Shenderova, Appl. Phys. Lett. **113**, 033105 (2018).

9. M. Bleija, O. Platnieks, J. Macutkevič, O. Starkova, S. Gaidukovs, Nanomaterials **12**, 3671 (2022).

10. J. Liu, H. B. Zhang, R. Sun, Y. Liu, A. Liu, A. Zhou, Z. Z. Yu, Advanced Materials **29**, 1702367 (2017).

11. M. Letellier, J. Macutkevic, P. Kuzhir, J. Banys, V. Fierro, A. Celzard, Carbon **122**, 217 (2017).

12. M. Letellier, J. Macutkevic, A. Paddubskaya, A. Plyushch, P. Kuzhir, M. Ivanov, J. Banys, A. Pizzi, V. Fierro, A. Celzard, IEEE Transactions on Electromagnetic Compatibility **57**, 989 (2015).

13. J. Castro-Gutiérrez, E. Palaimiene, J. Macutkevic, J. Banys, P. Kuzhir, S. Schaefer, V. Fierro, A. Celzard, Materials **12**, 4143 (2019).

14. C. H. Cui, D. X. Yan, H. Pang, L. C. Jia, X. Xu, S. Yang, J. Z. Xu, Z. M. Li, Chemical Engineering Journal 2017, 323, 29 (2017).

15. F. Jona, G. Shirane, Ferroelectric Crystals, Macmillan (1962).

16. X. Chen, G. Wang, Y. Duan, S. Liu, Journal of Alloys and Compounds **453**, 433 (2008).

17. P. Saini, M. Arora, G. Gupta, B. K. Gupta, V. N. Singh, V. Choudhary, Nanoscale **5**, 4330 (2013).

18. Y. Akinay, F. Hayat, Journal of Composite Materials **53**, 593 (2019).

19. N. Joseph, S. K. Singh, R. K. Sirugudu, V. R. K. Murthy, S. Ananthakumar, M. T. Sebastian, Materials Research Bulletin **48**, 1681 (2013).

20. Z. Guo, S. E. Lee, H. Kim, S. Park, H. T. Hahn, A. B. Karki, D. P. Young, Fabrication, Acta Materialia **57**, 267 (2009).

21. Z. Wang, K. Sun, P. Xie, Q. Hou, Y. Liu, Q. Gu, R. Fan, Acta Materialia **185**, 412 (2020).

22. A. Muzaffar, M. B. Ahamed, K. Deshmukh, M. Faisal, S.K.K. Pasha, Materials Letters **218**, 217 (2018).

23. G. Wang, X. Chen, Y. Duan, S. Liu, Journal of Alloys and Compounds **454**, 340 (2008).

24. A. P. Guo, X. J. Zhang, J. K. Qu, S. W. Wang, J. Q. Zhu, G. S. Wang, L. Guo, Mater. Chem. Front. **1**, 2519 (2017).

25. S. K. Singh, M. J. Akhtar, K. K. Kar, Composites Part B: Engineering **167**, 135 (2019).

26. L. Vovchenko, O. Lozitsky, L. Matzui, V. Oliynyk, V. Zagorodnii, M. Skoryk, Materials Chemistry and Physics **240**, 122234 (2020).

27. H. Wang, H. Ma, Nanotechnology **31**, 095711 (2019).

28. D. Xu, Y. Ren, X. Guo, B. Zhao, ACS Appl. Nano Mater. **5**, 14133 (2022).

29. P. Blyweert, V. Nicolas, J. Macutkevic, V. Fierro, A. Celzard, ACS Sustainable Chem. Eng. **10**, 7702 (2022).

30. P. Blyweert, V. Nicolas, V. Fierro, A. Celzard, Molecules **27**, 2091, 2022.

31. J. Grigas, *Microwave Dielectric Spectroscopy of Ferroelectrics and Related Materials* (Gordon and Breach Science Publishers, 1996).

32. A. Vaitkus, A. Merkys, S. Gražulis, J. Appl. Crystall. **54 (2)**, 661 (2021).

33. C. A. Klein, RMP **34**, 56 (1962).

34. L. F. Chen, C. K. Ong, C. P. Neo, V. V. Varadan, V. K. Varadan, Microwave electronics: measurement and materials characterization. John Wiley & Sons, 2004.

35. B. Wei, M. Wang, Z. Yao, Z. Chen, P. Chen, X. Tao, Y. Liu, J. Zhou, Carbon 191, 486 (2022).

36. R. L. Fante, M. T. McCormack, IEEE transactions on antennas and propagation **36**, 1443 (1988).

37. D. Meisak, A. Plyushch, J. Macutkevič, R. Grigalaitis, A. Sokal, K. N. Lapko, A. Selskis, P. P. Kuzhir, J. Banys, Journal of Materials Research and Technology **24**, 1939 (2023).

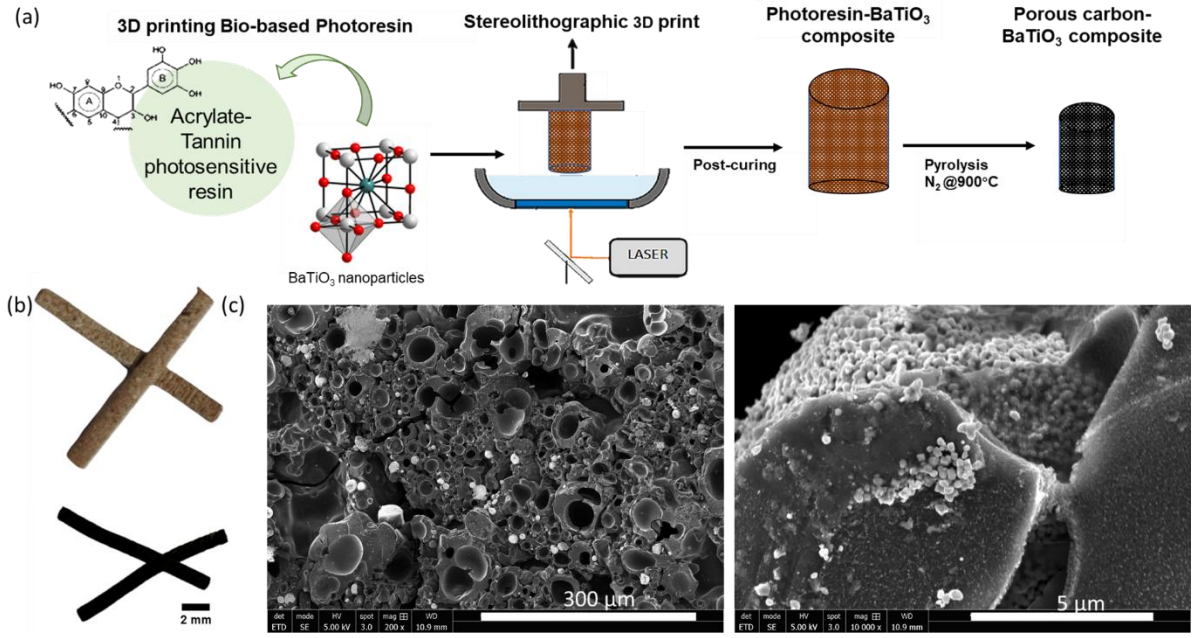


Figure 1(a) Schematic illustration of the fabrication strategy of porous carbon-$BaTiO_3$ composites; (b) Printed rods before (top) and after pyrolysis (bottom); and (c) typical SEM images of fractured carbon-BT composites.

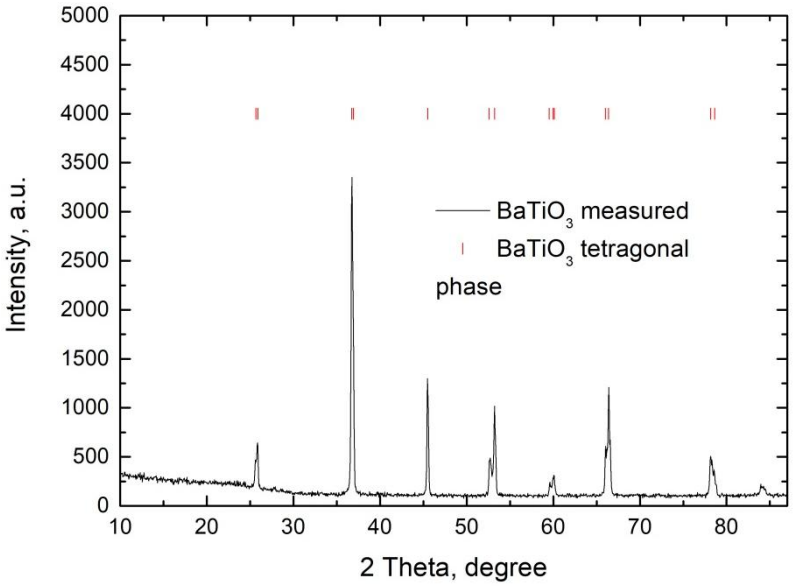


Figure 2. X-ray diffraction pattern of 200 nm $BaTiO_3$ nanoparticles.

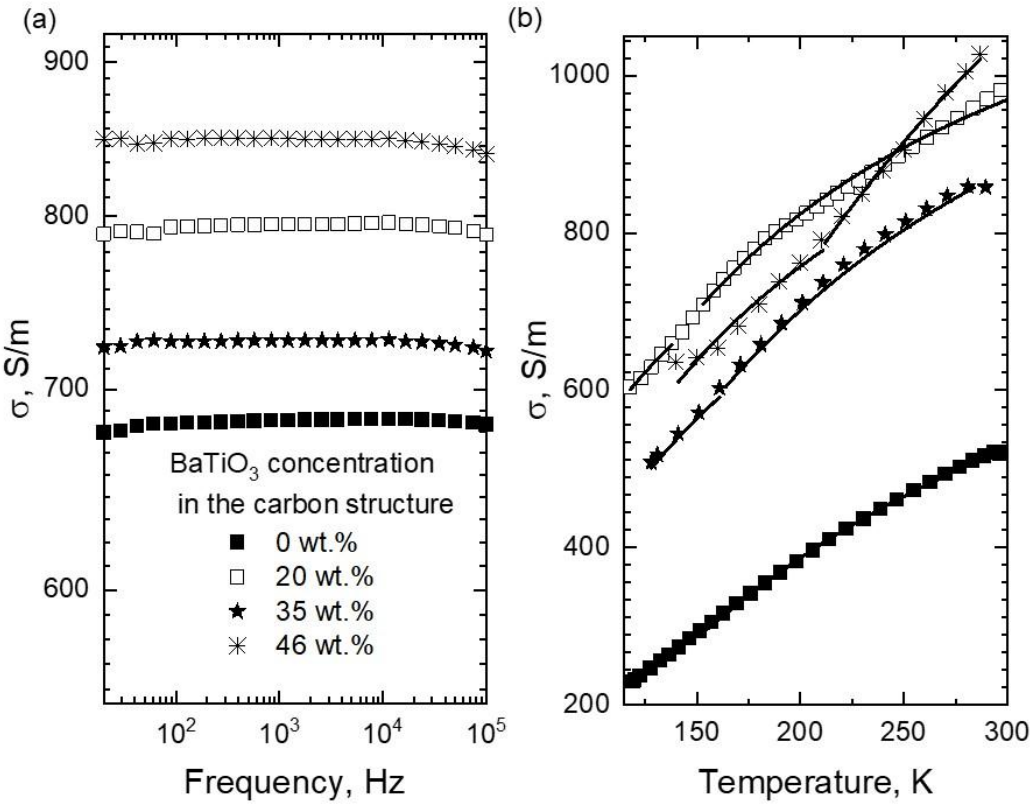


Figure 3. (a) Frequency dependence of electrical conductivity in the frequency range 20 Hz -1 MHz of carbon structures with different wt.% of $BaTiO_3$. (b) Temperature dependence of DC conductivity for the same samples. Solid lines are the best fit according to Arrhenius's law (Eq. 1).

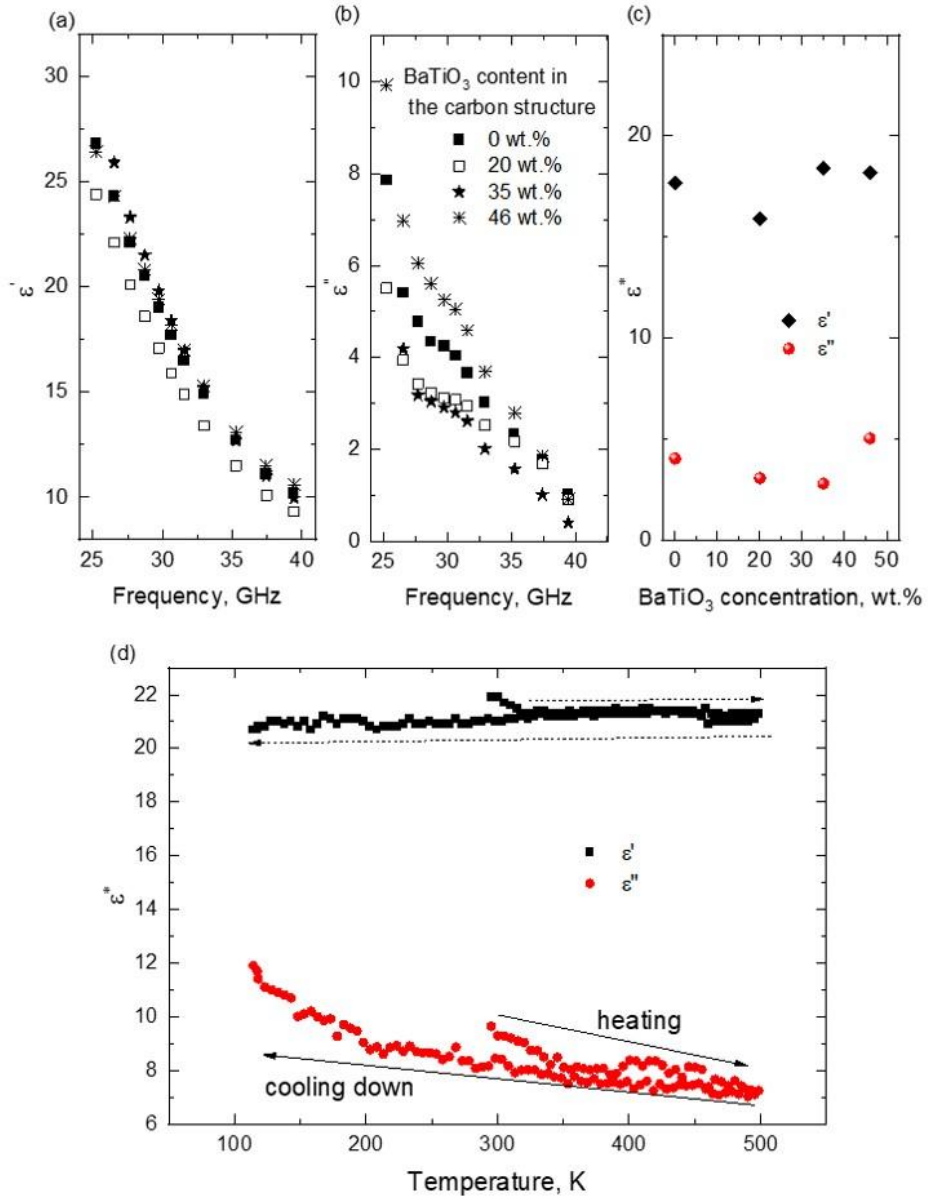


Figure 4. Frequency dependence of the prepared materials: (a) dielectric permittivity ε'; (b) dielectric losses ε''; (c) Complex dielectric permittivity of the composites as a function of $BaTiO_3$ concentration (wt.%); and (d) Temperature dependence of microwave dielectric properties at 27 GHz of structures without $BaTiO_3$. The error bars are smaller than the experimental points and therefore have not been added to the graph; the arrows indicate the direction of temperature change.

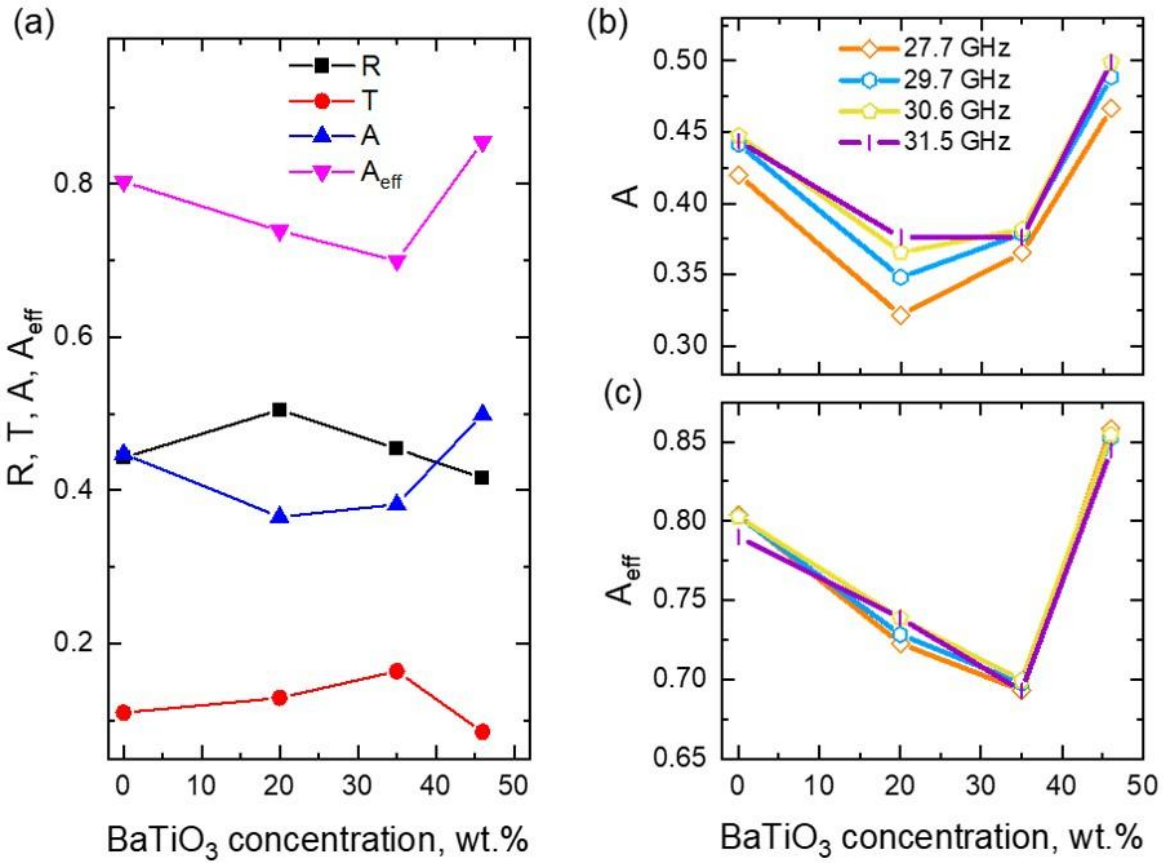


Figure 5. (a) Microwave properties (reflection R, transmission T, absorption A and effective absorption $A_{eff}$) of carbon structures as a function of $BaTiO_3$ concentration (wt.%) at 29.7 GHz; (b) Absorption of 2 mm-thick structures, as a function of the $BaTiO_3$ concentration for different frequencies; (c) Effective absorption of 2 mm-thick structures, as a function of $BaTiO_3$ concentration for different frequencies. The highest absorption is achieved at the highest BT concentration.

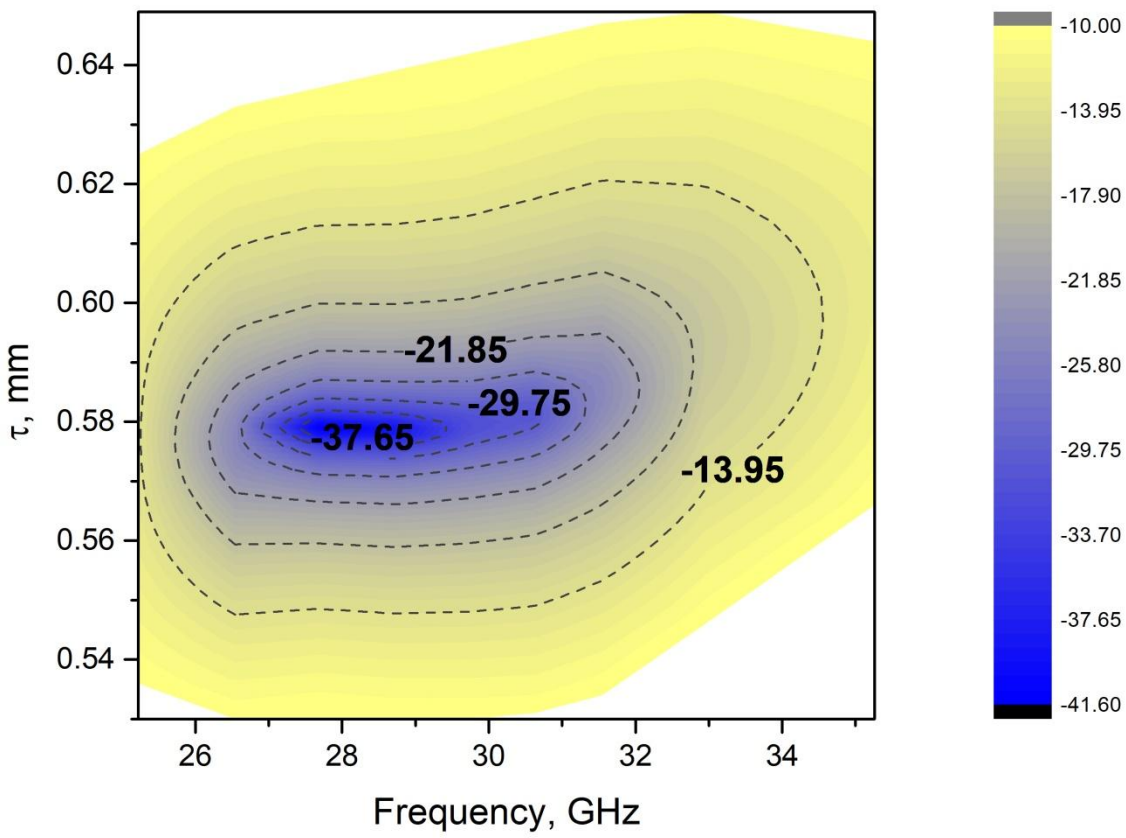


Figure 6. $S_{11}$ parameter of the sample layer containing 46 wt.% $BaTiO_3$ as a function of frequency and thickness.